Research Square

Preprints are preliminary reports that have not undergone peer review.
They should not be considered conclusive, used to inform clinical practice,
or referenced by the media as validated information.

Mineral Association State Regulates Microbial Contributions to Persistent Soil Carbon

Mengqiang Zhu

mqzhu@umd.edu

University of Maryland

Hongfei Liu

University of Maryland

Chao Liang

Institute of Applied Ecology https://orcid.org/0000-0002-9089-6546

Katerina Georgiou

Oregon State University

Article

Keywords: amino sugar, soil organic carbon, mineral-associated organic carbon, mineral protection, microbial-derived carbon, non-microbial carbon

Posted Date: June 3rd, 2026

DOI: https://doi.org/10.21203/rs.3.rs-9877881/v1

License: This work is licensed under a Creative Commons Attribution 4.0 International License.
Read Full License

Additional Declarations: There is **NO** Competing Interest.

Mineral Association State Regulates Microbial Contributions to Persistent Soil Carbon

Hongfei Liu[1], Chao Liang[2], Katerina Georgiou[3,4], and Mengqiang Zhu[1*]

[1]Department of Geological, Environmental, and Planetary Sciences, University of Maryland, College Park, MD 20742, USA

[2]State Key Laboratory for Development and Utilization of Forest Food Resource, College of Environmental and Resource Sciences, Zhejiang A&F University, Hangzhou 311300, China

[3]Department of Biological and Ecological Engineering, Oregon State University, Corvallis, Oregon, USA

[4]Physical and Life Sciences Directorate,Lawrence Livermore National Laboratory, Livermore, California, USA

* Corresponding author: Mengqiang Zhu

Abstract

Mineral association is a major mechanism of soil organic carbon (SOC) persistence, and mineral-associated organic carbon (MAOC) is often assumed to be preferentially derived from microbial residues. However, whether mineral association consistently favors microbial-derived over non-microbial carbon across environmental gradients remains unresolved. Here we combined continent-scale sampling of 192 soils from 43 U.S. National Ecological Observatory Network sites, horizon-resolved profiles to 2 m depth, size–density fractionation, and amino-sugar biomarkers to test how the realized degree of mineral association, indexed by the MAOC/SOC ratio, relates to carbon source allocation in bulk SOC and MAOC. We show that MAOC does not have a fixed microbial source identity. MAOC was not uniformly enriched in microbial-derived carbon relative to bulk SOC: this enrichment declined as MAOC/SOC increased, while non-microbial carbon became progressively enriched. Soil depth and chemical weathering were the strongest predictors of these source-specific enrichment patterns, and effective soil moisture shaped contrasting depth profiles in humid and arid systems. Our findings reveal mineral association state as a source-selective filter, challenging a uniform microbial-dominance model of MAOC formation and linking pedogenesis, hydrology, and vertical transport to persistent soil carbon formation across environmental gradients.

Keywords: amino sugar, soil organic carbon, mineral-associated organic carbon, mineral protection, microbial-derived carbon, non-microbial carbon

Introduction

Soil organic carbon (SOC) underpins terrestrial ecosystem functioning and modulates carbon-climate feedbacks [1,2]. Earlier frameworks emphasized plant-derived inputs, humified

organic matter and chemical recalcitrance as dominant controls on SOC persistence, whereas more recent concepts instead view SOC as a continuum of plant compounds, microbial products, and transformed residues whose persistence depends on their physicochemical environment [3–6]. Within this framework, SOC persistence is strongly shaped by its allocation between particulate organic carbon (POC) and mineral-associated organic carbon (MAOC), the latter being stabilized through interactions with mineral surfaces and generally exhibiting longer residence times [7–9]. A prevailing view is that minerals preferentially stabilize microbial-derived carbon over C of other sources because microbial residues are chemically reactive and can form strong mineral associations [10,11]. However, non-microbial carbon, much of it plant-derived, can also contribute substantially to MAOC, challenging a simple microbial-dominance model of MAOC formation [12–15]. Despite this progress, it remains unclear whether mineral association systematically alters the relative retention of microbial-derived versus non-microbial carbon within MAOC, and whether this source selectivity varies with the realized degree of mineral association of SOC.

A mechanistic explanation for this unresolved partitioning is that non-microbial and microbial-derived carbon may enter MAOC through distinct but coupled pathways. Non-microbial carbon may contribute to MAOC through direct sorption of low-molecular-weight dissolved organic carbon (DOC) onto mineral surfaces, making this pathway sensitive to mineral surface availability and mineral-solution chemistry [9,16,17]. By contrast, microbial-derived carbon, largely insoluble necromass, may enter MAOC through microbial processing and in vivo stabilization, including aggregation, cell–mineral contact, or other solid-phase interactions; this pathway may be less directly constrained by instantaneous sorptive surface area than DOC adsorption [17–19]. We propose that these contrasting pathways generate source-selective partitioning as the realized degree of mineral association changes. Where a larger proportion of SOC occurs as MAOC, direct incorporation of dissolved or root-derived carbon into mineral-associated pools may make a

74 greater relative contribution. Conversely, where a larger share of SOC remains outside MAOC,
75 particulate organic matter may accumulate and sustain microbial growth, promoting the transfer
76 of microbial products and necromass into MAOC [16,20,21]. We therefore hypothesized that the
77 realized degree of mineral association, indexed by MAOC/SOC, would be associated with shifts
78 in MAOC source composition: higher MAOC/SOC would correspond to greater relative
79 enrichment of non-microbial carbon in MAOC, whereas lower MAOC/SOC would correspond to
80 stronger microbial-derived carbon enrichment (Figure 1).

81 To test this hypothesis, we leveraged continent-scale sampling from the U.S. National
82 Ecological Observatory Network (NEON), analyzing 192 soil samples from 43 sites across broad
83 climatic, vegetation, and edaphic gradients, with soil profiles extending to 2 m depth. We isolated
84 MAOC using combined size–density fractionation and quantified amino sugars as biomarkers of
85 microbial-derived carbon in both bulk SOC and MAOC. We compared source composition
86 between MAOC and bulk SOC to assess the relative enrichment of microbial-derived versus non-
87 microbial carbon in MAOC. This design allowed us to test whether MAOC source composition
88 shifts systematically along a realized mineral-association gradient and whether these shifts are
89 linked to depth, weathering, and hydrological context.

90 **Results and Discussion**

91 **Degree of mineral association across soils**

92 The balance between SOC accumulation and MAOC formation varied predictably across
93 ecosystems, horizons, and soil textures. MAOC increased with SOC but at a diminishing rate
94 (Figure 2a), indicating that the apparent efficiency of MAOC formation declined as SOC
95 accumulated. Consequently, the degree of mineral association, quantified as MAOC/SOC,

decreased with increasing SOC (Figure 2b). Silt- and clay-rich soils attained higher MAOC concentrations than coarse-textured soils and therefore maintained higher MAOC/SOC ratios, consistent with the role of fine particles in supporting larger mineral-associated carbon pools [22,23].

We use MAOC/SOC as an empirical index of the realized degree of mineral association of SOC, but not as a direct measure of MAOC saturation. A high MAOC/SOC ratio can reflect greater mineral surface availability, lower SOC inputs, stronger decomposition of non-mineral-associated organic matter, or some combination of these factors. Similarly, a low MAOC/SOC ratio indicates that more SOC occurs outside the MAOC pool, but does not necessarily mean that MAOC is saturated. Because MAOC/SOC can also be shaped by texture, climate, vegetation, land use, management, decomposition, and ecosystem carbon input regimes, it is an imperfect proxy for saturation state [23–25]. We therefore interpret MAOC/SOC as a state variable describing SOC partitioning, while treating saturation-related mechanisms as interpretations that require independent information on mineral capacity and carbon loading.

Divergent enrichment of microbial and non-microbial C along the degree of mineral association

To determine whether mineral association selectively retains microbial-derived or non-microbial carbon, we first compared source contributions across SOC fractions and then quantified their enrichment in MAOC relative to bulk SOC. Across all samples, microbial-derived carbon accounted for, on average, 37.2% of MAOC (2.8–92.4%; n = 192), 34.4% of bulk SOC (3.1–97.1%; n = 192) and 10.8% of light particulate organic carbon (LPOC; 2.1–38.2%; n = 40) (Figure S2). The low microbial contribution in LPOC is consistent with the dominance of non-microbial, largely plant-derived carbon in this fraction. Mean microbial-derived carbon fractions in MAOC and SOC were lower than some synthesis-based estimates (17- 86%; mean = 48%) [12,26–28]. This

119 difference may partly reflect the inclusion of many deep soil samples in our dataset (Figure S4 and
120 S5), where substrate limitation and energetic constraints can suppress microbial turnover and
121 necromass production [29–31].

122 The relative microbial contribution to bulk SOC and MAOC changed only weakly with the
123 degree of mineral association. Increasing MAOC/SOC was associated with a greater relative
124 contribution of microbial-derived carbon to bulk SOC ($R^2 = 0.15$, $p < 0.001$, Figure S3a), but only
125 a negligible change in the microbial contribution to MAOC ($R^2 = 0.004$, $p = 0.009$, Figure S3b).
126 Non-microbial carbon showed the corresponding opposite pattern, with decreasing MAOC/SOC
127 associated with a greater relative contribution of non-microbial carbon to bulk SOC ($R^2 = 0.15$, p
128 < 0.001). These direct source fractions indicate that MAOC source composition is not fixed, but
129 they do not by themselves quantify whether MAOC is enriched or depleted in a given source
130 relative to bulk SOC.

131 We therefore calculated enrichment factors for microbial-derived carbon (EF_{MC}) and non-
132 microbial carbon (EF_{NMC}), which compare source-specific carbon density in MAOC with that in
133 bulk SOC. EF_{MC} ranged from −1.23 to 2.12 and EF_{NMC} from −2.44 to 2.75 (Figure 2c, d). The
134 enrichment pattern was not universal: 85 of 175 soils showed positive EF_{MC} and negative EF_{NMC},
135 indicating relative enrichment of microbial-derived carbon and depletion of non-microbial carbon
136 in MAOC, whereas 88 soils showed the opposite pattern. Thus, mineral-associated fractions did
137 not consistently favour microbial-derived over non-microbial carbon.

138 Because enrichment factors contain MAOC/SOC in their denominators, we tested whether
139 the observed trends exceeded the null expectation imposed by this algebraic structure. For EF_{MC},
140 a slope of −1 against ln(MAOC/SOC) would be expected if MC_{MAOM}/MC_{SOM} did not vary
141 systematically along the gradient. The observed slope was −0.75, significantly shallower than −1,
142 and $B_{MC} = \ln(MC_{MAOM}/MC_{SOM})$ increased significantly with ln(MAOC/SOC) (slope = 0.25, $R^2 =$

0.14, $p = 1.3\times10^{-6}$; Figure 2f). Thus, the decline in EF_{MC} was not a mathematical artifact; rather, microbial-derived carbon increasingly entered MAOM, but less than proportionally to total MAOC accumulation as MAOC/SOC increased. Additionally, the coupling-removed non-microbial signal, $B_{NMC} = \ln(NMC_{MAOM}/NMC_{SOM})$ increased even more strongly with ln(MAOC/SOC) (slope = 1.49, $R^2 = 0.77$, $p = 1.2\times10^{-51}$; Figure S6a). Consistently, the microbial-to-non-microbial log-ratio enrichment, $LR_{MC:NMC}$, declined significantly with ln(MAOC/SOC) (slope = −1.24, $R^2 = 0.50$, $p = 3.0\times10^{-25}$; Fig. S6b). This compositional test confirms that MAOC shifts from relative microbial enrichment at low MAOC/SOC toward relative non-microbial enrichment at high MAOC/SOC.

The enrichment patterns were not driven by the conversion factors used to estimate total microbial necromass carbon. Enrichment factors calculated separately for bacterial necromass carbon and fungal necromass carbon showed similar responses to MAOC/SOC (Figure S7), indicating that the EF_{MC} pattern was not an artifact of pooling bacterial and fungal necromass carbon.

We note that non-microbial carbon is operationally defined here as carbon not accounted for by amino-sugar-derived microbial necromass, because it was calculated by difference rather than measured directly as plant-derived carbon. Thus, although we interpret increasing non-microbial enrichment as consistent with greater plant-derived, dissolved, or root-derived contributions to MAOC, this source assignment remains inferential.

Together, the enrichment-factor and coupling-removed analyses indicate that microbial-derived and non-microbial carbon follow divergent enrichment trajectories along the mineral-association gradient. This pattern is consistent with independent chemical compositional analyses of the same MAOC samples, which showed that an adsorbed MAOC fraction was enriched in plant-derived dissolved organic carbon and exhibited Langmuir-type saturation behavior with

relatively low maximum loading, whereas an insoluble MAOC fraction, interpreted as more strongly influenced by microbial-derived carbon, continued to accumulate at higher rates and showed no clear evidence of saturation [17]. These complementary results suggest that non-microbial and microbial-derived carbon may enter MAOC through partly distinct pathways: direct sorption of dissolved plant-derived carbon where mineral surface availability is high, and microbial transformation or incorporation of particulate-derived carbon where carbon loading is greater. However, because the present study does not directly trace POC decomposition into microbial products or MAOC, this pathway remains an interpretation supported by prior work showing that decomposing particulate organic matter can sustain microbial growth and promote transfer of microbial products into mineral-associated pools [16,20,21].

Environmental controls on source-specific enrichment

Given the observed reciprocal shifts in EF_{MC} and EF_{NMC} along the MAOC/SOC gradient, we next examined which environmental factors were associated with variation in the realized degree of mineral association and source-specific enrichment across soils. Structural equation modelling identified soil depth and the chemical index of weathering (CIW) as the strongest predictors of MAOC/SOC, EF_{MC} and EF_{NMC} across ecosystems (Figure 3). Depth exerted the strongest total negative effect on $EF_{MC,}$ whereas CIW had the strongest positive associations with EF_{NMC} and MAOC/SOC. Soil effective moisture (MAP – PET) and mean annual temperature (MAT) were positively associated with CIW, suggesting that climate shaped source-specific enrichment partly through its association with chemical weathering (Figure 3a,c). Overall, deeper and more strongly weathered soils tended to have higher MAOC/SOC and EF_{NMC}, but lower EF_{MC}.

These relationships suggest that weathering and depth are linked to shifts in the dominant sources contributing to MAOC. Higher CIW likely reflects more advanced chemical weathering and greater abundance of reactive secondary minerals, including metal oxides [32–34]. In more weathered soils, greater reactive mineral availability, together with enhanced decomposition and production of low-molecular-weight dissolved organic compounds, may favor incorporation of non-microbial, dissolved or root-derived carbon into MAOC [35–39]. The associated decline in EF_{MC} should therefore not be interpreted as evidence for an absolute loss of microbial-derived carbon. Rather, it indicates weaker enrichment of microbial-derived carbon in MAOC relative to bulk SOC as non-microbial carbon makes a larger relative contribution to MAOC formation.

Depth-dependent input pathways and transport processes also appeared to regulate source enrichment. Surface soils generally receive larger particulate plant inputs and have higher SOC concentrations, conditions that can sustain microbial processing and promote microbial-derived carbon enrichment in MAOC. Deeper soils, by contrast, often have lower particulate inputs but proportionally greater influence of dissolved, root-derived, and vertically translocated carbon, as well as greater availability of reactive mineral surfaces. These conditions can increase the relative contribution of non-microbial carbon to MAOC and help explain the observed decline in EF_{MC} and increase in EF_{NMC} with depth.

Depth patterns of weathering, degree of mineral association, and source-specific enrichment differed strongly between humid and arid systems (Figure 4). In humid systems (MAP – PET: -16.9 – 1755 mm) , CIW and MAOC/SOC increased with depth, EF_{MC} declined, and EF_{NMC} increased monotonically (Figure 4a, c, e, g). This pattern is consistent with sustained percolation, deeper leaching, secondary mineral formation, and downward transport of dissolved or root-derived carbon [30,40]. In arid systems (MAP – PET: -1000 – -17 mm), by contrast, CIW, MAOC/SOC and EF_{NMC} peaked in the upper subsoil and declined with depth, whereas EF_{MC}

showed the opposite pattern (Figure 4b, d, f, h). This non-monotonic profile suggests that weathering and DOC transport are concentrated within the shallow zone reached by episodic wetting fronts, while deeper horizons remain less weathered and less connected to surface-derived DOC [40–42]. Below this shallow wetting-front zone, weaker weathering and reduced dissolved-carbon delivery may limit non-microbial contributions to MAOC, coinciding with higher EF_{MC} and lower EF_{NMC}.

Implications

Our findings advance a state-dependent view of soil carbon persistence. Mineral association is often treated primarily as a protective mechanism that increases carbon residence time, while the biological source of MAOC is frequently assumed to be relatively fixed or predominantly microbial [9–11]. Here, we show instead that the realized mineral-association state of SOC is associated with source-selective differences in MAOC composition. MAOC/SOC describes how SOC is partitioned between mineral-associated and non-mineral-associated pools, and this partitioning state was linked to shifts in the relative enrichment of microbial-derived versus non-microbial carbon. Thus, MAOC should be viewed not as a uniform stabilized pool, but as an emergent product of organic inputs, microbial processing, carbon loading, mineral surface availability, weathering, hydrology, and depth-dependent transport [3–6].

This perspective helps reconcile apparently conflicting views of MAOC formation. Microbial residues can be preferentially enriched in MAOC in many soils, consistent with the microbial efficiency–mineral stabilization framework [10,11]. However, this enrichment is not universal, and non-microbial carbon can also contribute substantially to MAOC [12,14,15]. Where a larger proportion of SOC occurs as MAOC, non-microbial dissolved or root-derived carbon may make a larger relative contribution through direct mineral association [17,35,43]. Where a larger share

of SOC remains outside MAOC, microbial transformation of particulate organic matter and incorporation of microbial products into mineral-associated pools may contribute more strongly to MAOC source enrichment [16,20,21]. The relevant question is therefore not whether MAOC is primarily microbial-derived or non-microbial-derived, but under what mineral-association state, depth, weathering regime, and hydrological context each source is preferentially retained.

For ecosystem and Earth system models, these findings indicate that representing MAOC as a homogeneous pool with fixed source composition or fixed formation efficiency is inadequate. Weathering, effective moisture, vertical transport, and soil depth do not merely regulate the size of MAOC pools; they also influence the pathways through which MAOC forms. As climate change alters plant productivity, microbial activity, precipitation regimes, and soil moisture dynamics, it may shift the source pathways feeding persistent soil carbon rather than simply changing total carbon inputs or decomposition rates [30,38,40]. Incorporating source-selective and state-dependent MAOC formation pathways could improve predictions of where persistent soil carbon accumulates, which biological sources contribute to it, and how soil carbon sequestration potential varies across environmental gradients under global change [8,24,25,38].

Methods

Study Sites and Sampling

We analyzed 192 bulk soils from 43 terrestrial sites within the National Ecological Observatory Network (NEON) (Figure S1). The sites span 20 ecoclimatic domains and encompass broad variation in landforms, vegetation, climate, and ecosystem processes across the United States. At each site, NEON excavated a single temporary pit ("Megapit") positioned to represent

the dominant soil, vegetation, and topographic setting around the site's flux tower, thereby aligning the soil archive with nearby sensor footprints. Soils were sampled by genetic horizon to depths of ≤2 m in non-permafrost regions and ≤3 m at Alaskan sites, following standardized NEON protocols for field sampling and laboratory analyses to minimize sampling and analytical bias. For Gelisols with extensive O horizons, we targeted the first two mineral sub-horizons for analysis (e.g., Cgjj/Oajj and Cgjff/Oajjf at BARR; Bg/Oajj and Cg at BONA; A/Cjj and Cjjf at HEAL; Bw and BC at TOOL). Although the Megapit design lacks within-site replication, prior work demonstrates that Megapit archives capture major spatial patterns in SOC and MAOC at continental scales [40,44–46]. Accordingly, our site-level inferences emphasize cross-site gradients rather than within-site variability.

Soil physical and chemical properties and environmental covariates

Organic carbon (OC) and total nitrogen (TN) in bulk soil, light POM (LPOM), and MAOM were measured with an elemental analyzer. For carbonate-bearing soils (pH > 6.0), inorganic carbon in bulk soil and MAOM was removed by HCl fumigation prior to OC determination [47]. Oxalate-extractable Fe and Al—indexing short-range-order (SRO) phases and organo-metal complexes (termed Feox and Alox)—were obtained by ammonium oxalate extraction and quantified by inductively coupled plasma optical emission spectroscopy (ICP–OES) [48].

Site-level soil physicochemical data were obtained from the NEON data portal using horizon-resolved Megapit measurements. Particle-size data included total sand, silt, and clay fractions, as well as sand and silt subclasses: very fine sand, fine sand, medium sand, coarse sand, very coarse sand, fine silt, and coarse silt. Chemical variables included total concentrations of C, N, S, Al, Ca, Fe, K, Mg, Mn, Na, P and Si, pH, electrical conductivity, gypsum and carbonate

contents, ammonium-acetate–extractable Ca, K, Mg, and Na, cation exchange capacity, and KCl-extractable Al and Mn. CIW was calculated as:

$$\mathrm{CIW} = 100 \times \frac{\mathrm{Al_2O_3}}{\mathrm{Al_2O_3} + \mathrm{CaO^*} + \mathrm{Na_2O}}$$

where oxides are expressed in molar units and $\mathrm{CaO^*}$ represents Ca in silicate minerals after correction for carbonate- and phosphate-associated Ca. If carbonate-corrected Ca was unavailable, we calculated CIW using total Ca and interpret CIW as an apparent weathering index.

Litterfall data were compiled from elevated PVC litter traps with a 0.5 m² aperture across 33 NEON sites: ABBY, BART, BLAN, BONA, CLBJ, DEJU, DELA, GRSM, GUAN, HARV, HEAL, JERC, KONZ, LENO, MLBS, NIWO, ORNL, OSBS, PUUM, RMNP, SCBI, SERC, SJER, SOAP, SRER, STEI, TALL, TEAK, TREE, UKFS, UNDE, WREF, and YELL. Dry mass was reported as total litterfall and by functional group, including seeds, needles, twigs or branches, woody material, flowers, leaves, mixed material, and other material.

Root biomass data were obtained from the NEON data portal for three soil profiles per Megapit at all sites except KONA and TOOL. Because NEON root biomass measurements are reported in 10-cm depth increments, whereas soils in this study were sampled by genetic horizon, horizon boundaries were rounded to the nearest 10 cm to align the datasets. Root biomass values from all depth bins overlapping each adjusted horizon interval were aggregated to estimate horizon-level biomass, and estimates were then averaged across the three profiles at each site.

Mean annual temperature (MAT) was obtained from the NEON data portal. Mean annual precipitation (MAP) and potential evapotranspiration (PET) were generated using ClimateNA v5.10 [49], with PET calculated using the temperature-based Hargreaves method.

Physical Fractionation of Soil Organic Matter

A subset of 192 soil samples from 43 sites was used for physical fractionation of soil organic matter (SOM) and for quantifying amino sugar in mineral-associated organic matter (MAOM). Soil organic matter was separated into LPOM, heavy particulate organic matter (HPOM), and MAOM using a combined density (sodium polytungstate, 1.85 g cm^{-3}) and size (53 μm) fractionation protocol [50]. Approximately 5 g of air-dried (<2 mm) soil was shaken with deionized water for 15 min and centrifuged at 5,000 rpm for 30 min. The supernatant was filtered through a 0.45 μm PTFE membrane to remove water-extractable organic matter. The particulates (size >0.45 μm) captured on the membrane were returned to the residual soil. Twelve glass beads and 25 ml of sodium polytungstate (1.85 g cm^{-3}) were added to the soil residue, which was shaken for 18 h to disperse soil aggregates and then centrifuged at 5,000 rpm for 30 min. The resulting LPOM fraction (density <1.85 g cm^{-3}) was decanted, rinsed thoroughly with deionized water to remove salts. The heavy pellet (density >1.85 g cm^{-3}) was repeatedly rinsed to remove residual sodium polytungstate and wet-sieved at 53 μm to separate HPOM (density >1.85 g cm^{-3} and size >53 μm) from MAOM (density >1.85 g cm^{-3} and size <53 μm). All fractions (LPOM, HPOM, MAOM) were oven-dried at 60 °C and gently ground to fine powders prior to biochemical analyses.

Amino-sugar analysis and microbial necromass carbon calculations

All 192 bulk and MAOM samples were measured for concentrations of amino sugars, including glucosamine (GlcN) and muramic acid (MurA). Only 42 LPOM samples from 33 NEON sites were measured because LPOM yields were frequently too small to meet the minimum mass required for amino sugar measurement. HPOM was not measured due to the low C concentration. Amino sugar concentrations in these samples were quantified following Zhang and Amelung, 1996, which used aldonitrile acetate derivatization and gas chromatography (GC).

Aliquots of soil samples (finely ground, <150 μm) containing ~0.3 mg N were placed in sealed hydrolysis vials, treated with 6 M HCl at 105 °C for 8 h, and cooled. The hydrolysates were amended with myo-inositol (internal standard), filtered, and concentrated to dryness. After neutralization to pH 6.6–6.8, samples were centrifuged and the supernatants freeze-dried. Residues were dissolved in methanol, evaporated under N_2, re-dissolved in deionized water, amended with a second internal standard (methylglucamine), and freeze-dried. Derivatization to aldonitrile acetates was performed with hydroxylamine hydrochloride and 4-(dimethylamino)pyridine in a 4:1 (v/v) pyridine–methanol mixture at 80 °C for 30 min, followed by acetylation with acetic anhydride at 80 °C for 60 min. After cooling, dichloromethane and 1 M HCl were added; excess reagents were removed by aqueous washing, and the organic phase was dried under N_2. Derivatives were reconstituted in solvent and analyzed by GC equipped with a DB-5 capillary column (60 m × 0.25 mm × 0.25 μm) to resolve amino-sugar derivatives.

Microbial necromass carbon was estimated from glucosamine and muramic acid concentrations [26,52]. Bacterial necromass carbon was calculated as: Bacterial necromass carbon = MurA × 45. Fungal necromass carbon was calculated as: Fungal necromass carbon = (GlcN/179.17 – 2 × MurA/251.23) × 179.17 × 9. Total microbial necromass carbon equals the sum of bacterial and fungal necromass carbon. Here, 45 converts MurA to bacterial necromass carbon; 179.17 and 251.23 are the molecular masses (g mol^{-1}) of GlcN and MurA, respectively; and 9 converts fungal GlcN to fungal necromass carbon.

Enrichment factor of microbial- and non-microbial-derived carbon

To evaluate whether mineral association selectively enriched microbial-derived or non-microbial carbon, we calculated enrichment factors comparing the carbon-source density of

MAOC with that of bulk SOC. Microbial-derived carbon was estimated from amino sugar biomarkers as described above. Non-microbial carbon was calculated by difference:

$$\mathrm{NMC_{MAOM}} = \mathrm{MAOC} - \mathrm{MC_{MAOM}}$$

$$\mathrm{NMC_{SOM}} = \mathrm{SOC} - \mathrm{MC_{SOM}}$$

where $\mathrm{MC_{MAOM}}$ and $\mathrm{MC_{SOM}}$ denote microbial-derived carbon in MAOM and bulk SOM, respectively, and $\mathrm{NMC_{MAOM}}$ and $\mathrm{NMC_{SOM}}$ denote non-microbial carbon in the corresponding pools.

The microbial-carbon enrichment factor was defined as:

$$EF_{\mathrm{MC}} = \ln\left(\frac{\mathrm{MC_{MAOM}}/\mathrm{MAOC}}{\mathrm{MC_{SOM}}/\mathrm{SOC}}\right)$$

and the non-microbial-carbon enrichment factor was defined as:

$$EF_{\mathrm{NMC}} = \ln\left(\frac{\mathrm{NMC_{MAOM}}/\mathrm{MAOC}}{\mathrm{NMC_{SOM}}/\mathrm{SOC}}\right)$$

Positive EF_{MC} values indicate that microbial-derived carbon is enriched in MAOC relative to bulk SOC, whereas negative EF_{MC} values indicate depletion. Positive EF_{NMC} values indicate enrichment of non-microbial carbon in MAOC relative to bulk SOC, whereas negative values indicate depletion. Because NMC was calculated by difference, we interpret non-microbial carbon primarily as carbon not accounted for by amino-sugar-derived microbial necromass estimates, rather than as a direct measurement of plant-derived carbon.

The enrichment factors can be decomposed algebraically as:

$$EF_{\mathrm{MC}} = \ln\left(\frac{\mathrm{MC_{MAOM}}}{\mathrm{MC_{SOM}}}\right) - \ln\left(\frac{\mathrm{MAOC}}{\mathrm{SOC}}\right)$$

$$EF_{\mathrm{NMC}} = \ln\left(\frac{\mathrm{NMC_{MAOM}}}{\mathrm{NMC_{SOM}}}\right) - \ln\left(\frac{\mathrm{MAOC}}{\mathrm{SOC}}\right)$$

This decomposition shows that both enrichment factors contain $-\ln(\mathrm{MAOC}/\mathrm{SOC})$ by definition. Therefore, regressions of enrichment factors against $\ln(\mathrm{MAOC}/\mathrm{SOC})$ can include an

algebraically imposed negative component. To separate this definitional dependence from biological source partitioning, we also calculated coupling-removed terms:

$$B_{MC} = \ln\left(\frac{MC_{MAOM}}{MC_{SOM}}\right) = EF_{MC} + \ln\left(\frac{MAOC}{SOC}\right)$$

$$B_{NMC} = \ln\left(\frac{NMC_{MAOM}}{NMC_{SOM}}\right) = EF_{NMC} + \ln\left(\frac{MAOC}{SOC}\right)$$

The B_{MC} and B_{NMC} terms quantify how much microbial-derived and non-microbial carbon, respectively, occur in MAOM relative to bulk SOM without directly retaining the $-\ln(MAOC/SOC)$ term embedded in the enrichment-factor definitions.

As an additional source-composition metric independent of the common $MAOC/SOC$ denominator, we calculated the microbial-to-non-microbial log-ratio enrichment of MAOC relative to bulk SOM:

$$LR_{MC:NMC} = \ln\left(\frac{MC_{MAOM}/NMC_{MAOM}}{MC_{SOM}/NMC_{SOM}}\right)$$

This metric is equivalent to $EF_{MC} - EF_{NMC}$ and tests whether MAOC is enriched in microbial-derived carbon relative to non-microbial carbon compared with bulk SOC.

Statistical analyses

To examine source enrichment along the degree of mineral association, we expressed $MAOC/SOC$ as a fraction and used its natural logarithm, $\ln(MAOC/SOC)$, as the mineral-association gradient. We first regressed EF_{MC} and EF_{NMC} against $\ln(MAOC/SOC)$ using ordinary least squares. Because both enrichment factors contain $-\ln(MAOC/SOC)$ by definition, a slope of -1 is expected if the numerator terms, B_{MC} or B_{NMC}, do not vary systematically with mineral association. We therefore tested whether the observed slopes of EF_{MC} and EF_{NMC} differed from -1 using two-sided t-tests:

$$t = \frac{\hat{\beta} + 1}{SE(\hat{\beta})}$$

where $\hat{\beta}$ is the fitted slope of the enrichment factor against $\ln(\mathrm{MAOC}/\mathrm{SOC})$. We also tested whether the slopes differed from zero to evaluate the overall direction and strength of enrichment-factor change.

To remove the algebraic coupling directly, we regressed B_{MC} and B_{NMC} against $\ln(\mathrm{MAOC}/\mathrm{SOC})$. A nonzero slope for B_{MC} or B_{NMC} indicates that source partitioning into MAOM changes along the mineral-association gradient beyond the definitional dependence embedded in the enrichment factors. We also regressed $LR_{MC:NMC}$ against $\ln(\mathrm{MAOC}/\mathrm{SOC})$ as a compositional log-ratio test of whether MAOC became relatively enriched or depleted in microbial-derived carbon compared with non-microbial carbon.

Sign-reversal points were estimated as the $\mathrm{MAOC}/\mathrm{SOC}$ value at which an enrichment factor equals zero. For each fitted enrichment-factor model,

$$\mathrm{EF} = \alpha + \beta \ln(\mathrm{MAOC}/\mathrm{SOC})$$

the sign-reversal point was calculated as:

$$\mathrm{MAOC}/\mathrm{SOC} = \exp\left(-\frac{\alpha}{\beta}\right)$$

Confidence intervals for sign-reversal points were estimated using 5,000 bootstrap resamples. Because multiple horizons were sampled within sites, bootstrap resampling was conducted at the site level when evaluating cross-site relationships.

To evaluate whether enrichment-factor relationships were robust to site structure and environmental covariates, we fit mixed-effects models with site as a random intercept:

$$\mathrm{Response} \sim \ln(\mathrm{MAOC}/\mathrm{SOC}) + \mathrm{Depth} + \mathrm{CIW} + \mathrm{MAT} + (\mathrm{MAP} - \mathrm{PET}) + \mathrm{Texture} + \cdots + (1 \mid \mathrm{Site})$$

where Response included EF_{MC}, EF_{NMC}, B_{MC}, B_{NMC}, and $LR_{MC:NMC}$. Predictor sets were screened for multicollinearity using variance inflation factors (VIF), and variables with VIF > 5 were removed before model fitting. We also conducted sensitivity analyses by fitting models separately for surface and subsoil horizons, humid and arid sites, and by sequentially excluding individual NEON domains or sites. These analyses were used to determine whether the enrichment patterns were driven by a small subset of sites, depth intervals, or climate regimes.

To assess the influence of amino-sugar conversion factors, enrichment analyses were repeated separately for bacterial necromass carbon and fungal necromass carbon. Bacterial and fungal enrichment factors were calculated using the same enrichment-factor structure as above, replacing total microbial-derived carbon with bacterial- or fungal-derived carbon. This analysis tested whether the main enrichment patterns depended on the conversion factors used to combine bacterial and fungal necromass into total microbial necromass carbon.

For environmental controls on source-specific enrichment, we constructed structural equation models using the piecewiseSEM package in R to estimate direct and indirect associations among environmental variables, MAOC/SOC, EF_{MC}, and EF_{NMC}. Candidate predictors included soil depth, chemical index of weathering (CIW), climate variables, texture, vegetation attributes, and soil physicochemical properties. Depth-dependent patterns in MAOC/SOC, EF_{MC}, EF_{NMC}, B_{MC}, B_{NMC}, $LR_{MC:NMC}$, CIW, MC_{MAOM}/MAOC, and MC_{SOM}/SOC were explored using locally weighted regression (LOESS). Before fitting depth profiles, soil depth and response variables were normalized within sites to reduce the influence of site-specific ranges and improve comparability among profiles. All statistical analyses were conducted in R.

Acknowledgements

C.L. acknowledges funding support from the National Natural Science Foundation of China (Grant No. 32241037). M.Z. and H.L. acknowledge support by a grant #NR233A750004G008 from the United States Department of Agriculture Climate Smart Commodities funding. Any opinions, findings, and conclusions or recommendations expressed in this material are those of the author(s) and do not necessarily reflect the views of and are not explicitly or implicitly promoted or endorsed by the United States Department of Agriculture. The National Ecological Observatory Network (NEON) is a program sponsored by the U.S. National Science Foundation and operated under cooperative agreement by Battelle under Cooperative Agreement No. 2346114. This material uses specimens and/or samples collected as part of the NEON Program.

Author contributions

M.Z. and H.L.: conceptualization and study design. H.L.: investigation, data collection, formal analysis, and visualization. C.L.: data collection and conceptual development. K.G.: conceptual development and interpretation. H.L. and M.Z.: writing original draft. All authors contributed to writing - review and editing and approved the final manuscript.

Competing interests

Authors declare that they have no competing interests.

References

1. Bot, A. & Benites, J. *The Importance of Soil Organic Matter: Key to Drought-Resistant Soil and Sustained Food Production*. vol. 80 (Food & Agriculture Org., 2005).

2. Cotrufo, M. F. & Lavallee, J. M. Chapter One - Soil organic matter formation, persistence, and functioning: A synthesis of current understanding to inform its conservation and regeneration. in *Advances in Agronomy* (ed. Sparks, D. L.) vol. 172 1–66 (Academic Press, 2022).

3. Miltner, A., Bombach, P., Schmidt-Brücken, B. & Kästner, M. SOM genesis: microbial biomass as a significant source. *Biogeochemistry* **111**, 41–55 (2012).

4. Lehmann, J. & Kleber, M. The contentious nature of soil organic matter. *Nature* **528**, 60–68 (2015).

5. Liang, C., Schimel, J. P. & Jastrow, J. D. The importance of anabolism in microbial control over soil carbon storage. *Nature Microbiology* **2**, 17105 (2017).

6. Schmidt, M. W. I. *et al.* Persistence of soil organic matter as an ecosystem property. *Nature* **478**, 49–56 (2011).

7. Torn, M. S., Trumbore, S. E., Chadwick, O. A., Vitousek, P. M. & Hendricks, D. M. Mineral control of soil organic carbon storage and turnover. *Nature* **389**, 170–173 (1997).

8. Zhou, Z. *et al.* Global turnover of soil mineral-associated and particulate organic carbon. *Nature Communications* **15**, 5329 (2024).

9. Lavallee, J. M., Soong, J. L. & Cotrufo, M. F. Conceptualizing soil organic matter into particulate and mineral-associated forms to address global change in the 21st century. *Global Change Biology* **26**, 261–273 (2020).

10. Cotrufo, M. F., Wallenstein, M. D., Boot, C. M., Denef, K. & Paul, E. The Microbial Efficiency-Matrix Stabilization (MEMS) framework integrates plant litter decomposition with soil organic matter stabilization: do labile plant inputs form stable soil organic matter? *Global Change Biology* **19**, 988–995 (2013).

11. Kallenbach, C. M., Frey, S. D. & Grandy, A. S. Direct evidence for microbial-derived soil organic matter formation and its ecophysiological controls. *Nature Communications* **7**, 13630 (2016).

12. Angst, G., Mueller, K. E., Nierop, K. G. J. & Simpson, M. J. Plant- or microbial-derived? A review on the molecular composition of stabilized soil organic matter. *Soil Biology and Biochemistry* **156**, 108189 (2021).

13. Angst, G. *et al.* Conceptualizing soil fauna effects on labile and stabilized soil organic matter. *Nature Communications* **15**, 5005 (2024).

14. Kramer, M. G., Sanderman, J., Chadwick, O. A., Chorover, J. & Vitousek, P. M. Long-term carbon storage through retention of dissolved aromatic acids by reactive particles in soil. *Global Change Biology* **18**, 2594–2605 (2012).

15. Sokol, N. W. *et al.* The path from root input to mineral-associated soil carbon is dictated by habitat-specific microbial traits and soil moisture. *Soil Biology and Biochemistry* **193**, 109367 (2024).

16. Cotrufo, M. F. *et al.* Formation of soil organic matter via biochemical and physical pathways of litter mass loss. *Nature Geoscience* **8**, 776–779 (2015).

17. Liu, H. *et al.* Dual and divergent formation pathways govern the composition and origins of mineral-associated organic carbon. *EarthArXiv* (2025).

18. Sokol, N. W., Sanderman, J. & Bradford, M. A. Pathways of mineral-associated soil organic matter formation: Integrating the role of plant carbon source, chemistry, and point of entry. *Global Change Biology* **25**, 12–24 (2019).

19. Sokol, N. W. & Bradford, M. A. Microbial formation of stable soil carbon is more efficient from belowground than aboveground input. *Nature Geoscience* **12**, 46–53 (2019).

20. Vidal, A. *et al.* Visualizing the transfer of organic matter from decaying plant residues to soil mineral surfaces controlled by microorganisms. *Soil Biology and Biochemistry* **160**, 108347 (2021).

21. Witzgall, K. *et al.* Particulate organic matter as a functional soil component for persistent soil organic carbon. *Nature Communications* **12**, 4115 (2021).

22. Begill, N., Don, A. & Poeplau, C. No detectable upper limit of mineral-associated organic carbon in temperate agricultural soils. *Global Change Biology* **29**, 4662–4669 (2023).

23. Georgiou, K. *et al.* Soil Carbon Saturation: What Do We Really Know? *Global Change Biology* **31**, e70197 (2025).

24. Cotrufo, M. F., Ranalli, M. G., Haddix, M. L., Six, J. & Lugato, E. Soil carbon storage informed by particulate and mineral-associated organic matter. *Nature Geoscience* **12**, 989–994 (2019).

25. Georgiou, K. *et al.* Global stocks and capacity of mineral-associated soil organic carbon. *Nature Communications* **13**, 3797 (2022).

26. Liang, C., Amelung, W., Lehmann, J. & Kästner, M. Quantitative assessment of microbial necromass contribution to soil organic matter. *Global change biology* **25**, 3578–3590 (2019).

27. Hu, H. *et al.* Reducing the uncertainty in estimating soil microbial-derived carbon storage. *Proceedings of the National Academy of Sciences* **121**, e2401916121 (2024).

28. Xuan, M., Ai, L., Wu, F., Zhang, X. & Ni, X. Biomarkers evidence shows a preferential occlusion of microbial necromass in mineral-associated and not particle organic matter. *Geoderma* **450**, 117030 (2024).

29. Fontaine, S. *et al.* Stability of organic carbon in deep soil layers controlled by fresh carbon supply. *Nature* **450**, 277–280 (2007).

30. Rumpel, C. & Kögel-Knabner, I. Deep soil organic matter—a key but poorly understood component of terrestrial C cycle. *Plant and Soil* **338**, 143–158 (2011).

31. Ahrens, B. *et al.* Combination of energy limitation and sorption capacity explains 14C depth gradients. *Soil Biology and Biochemistry* **148**, 107912 (2020).

32. Sheldon, N. D., Retallack, G. J. & Tanaka, S. Geochemical Climofunctions from North American Soils and Application to Paleosols across the Eocene-Oligocene Boundary in Oregon. *The Journal of Geology* **110**, 687–696 (2002).

33. Maher, K. & Chamberlain, C. P. Hydrologic Regulation of Chemical Weathering and the Geologic Carbon Cycle. *Science* **343**, 1502–1504 (2014).

34. Slessarev, E. W., Chadwick, O. A., Sokol, N. W., Nuccio, E. E. & Pett-Ridge, J. Rock weathering controls the potential for soil carbon storage at a continental scale. *Biogeochemistry* **157**, 1–13 (2022).

35. Kaiser, K. & Guggenberger, G. The role of DOM sorption to mineral surfaces in the preservation of organic matter in soils. *Organic geochemistry* **31**, 711–725 (2000).

36. Kleber, M. *et al.* Chapter One - Mineral–Organic Associations: Formation, Properties, and Relevance in Soil Environments. in *Advances in Agronomy* (ed. Sparks, D. L.) vol. 130 1–140 (Academic Press, 2015).

37. Lugato, E., Lavallee, J., Haddix, M., Panagos, P. & Cotrufo, M. Different climate sensitivity of particulate and mineral-associated soil organic matter. *NATURE GEOSCIENCE* **14**, 295-+ (2021).

38. Georgiou, K. *et al.* Emergent temperature sensitivity of soil organic carbon driven by mineral associations. *Nature Geoscience* **17**, 205–212 (2024).

39. Li, X. *et al.* Effects of mineral adsorption on the molecular composition of soil dissolved organic matter: Evidence from spectral analyses. *Chemical Geology* **669**, 122352 (2024).

40. Heckman, K. A. *et al.* Moisture-driven divergence in mineral-associated soil carbon persistence. *Proceedings of the National Academy of Sciences* **120**, e2210044120 (2023).

41. Hagedorn, F. & Joos, O. Experimental summer drought reduces soil CO2 effluxes and DOC leaching in Swiss grassland soils along an elevational gradient. *Biogeochemistry* **117**, 395–412 (2014).

42. Fan, Y. & Miguez-Macho, G. Infiltration depth, rooting depth, and regolith flushing—A global perspective. *PNAS Nexus* **3**, pgae514 (2024).

43. Kaiser, K. & Kalbitz, K. Cycling downwards – dissolved organic matter in soils. *Soil Biology and Biochemistry* **52**, 29–32 (2012).

44. Kramer, M. G. & Chadwick, O. A. Climate-driven thresholds in reactive mineral retention of soil carbon at the global scale. *Nature Climate Change* **8**, 1104–1108 (2018).

45. Hall, S. J., Ye, C., Weintraub, S. R. & Hockaday, W. C. Molecular trade-offs in soil organic carbon composition at continental scale. *Nature Geoscience* **13**, 687–692 (2020).

46. Nave, L. E. *et al.* Patterns and predictors of soil organic carbon storage across a continental-scale network. *Biogeochemistry* **156**, 75–96 (2021).

47. Harris, D., Horwáth, W. R. & van Kessel, C. Acid fumigation of soils to remove carbonates prior to total organic carbon or CARBON-13 isotopic analysis. *Soil Science Society of America Journal* **65**, 1853–1856 (2001).

48. Ross, G. & Wang, C. Extractable Al, Fe, Mn, and Si. *Soil sampling and methods of analysis* **1993**, 239–246 (1993).

49. Wang, T., Hamann, A., Spittlehouse, D. & Carroll, C. Locally Downscaled and Spatially Customizable Climate Data for Historical and Future Periods for North America. *PLOS ONE* **11**, e0156720 (2016).

50. Leuthold, S., Lavallee, J. M., Haddix, M. L. & Cotrufo, M. F. Contrasting properties of soil organic matter fractions isolated by different physical separation methodologies. *Geoderma* **445**, 116870 (2024).

51. Zhang, X. & Amelung, W. Gas chromatographic determination of muramic acid, glucosamine, mannosamine, and galactosamine in soils. *Soil Biology and Biochemistry* **28**, 1201–1206 (1996).

52. Appuhn, A. & Joergensen, R. G. Microbial colonisation of roots as a function of plant species. *Soil Biology and Biochemistry* **38**, 1040–1051 (2006).

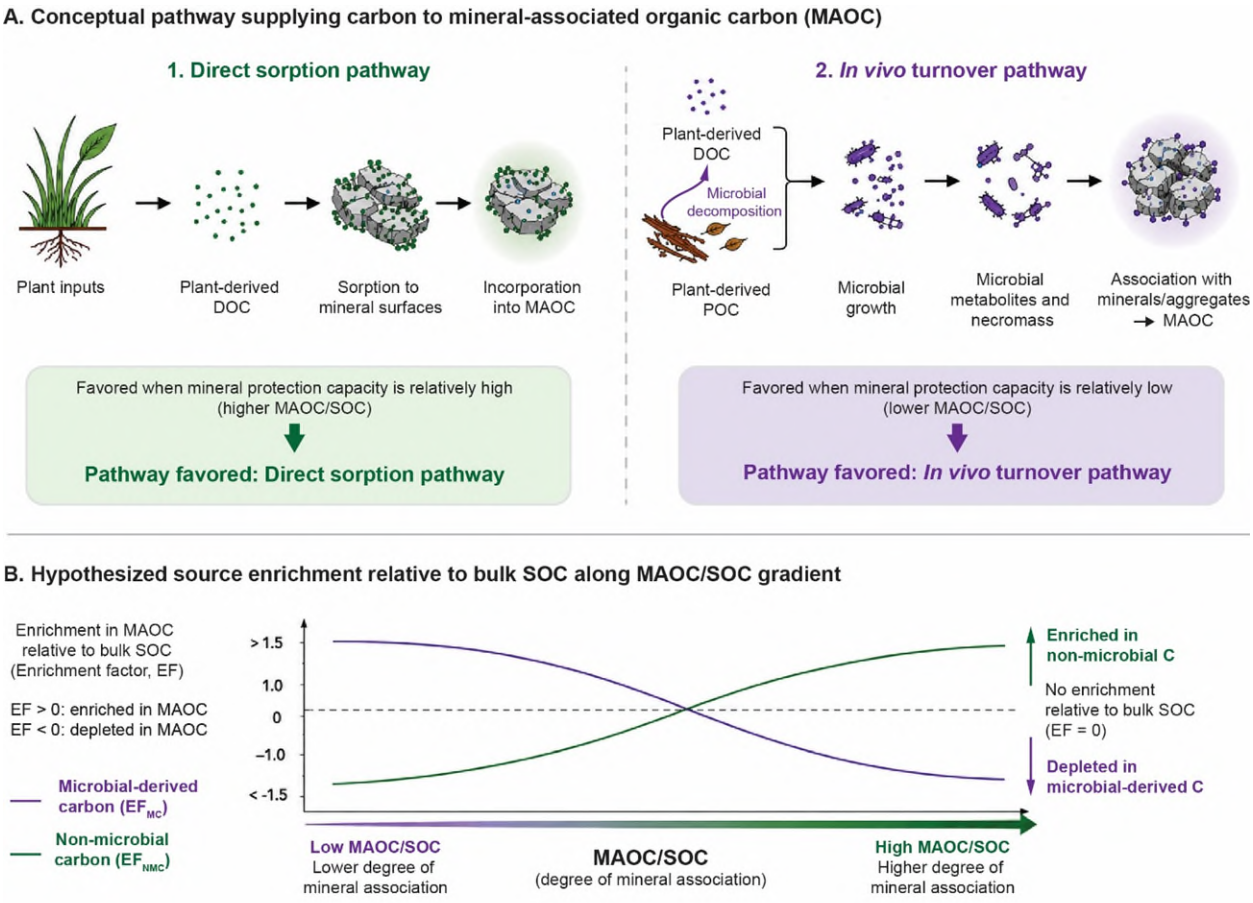


Fig. 1 | Conceptual model of source-selective mineral association. Microbial-derived and non-microbial carbon can enter mineral-associated organic carbon through distinct but coupled pathways. At lower MAOC/SOC, non-microbial carbon accumulates more as particulate organic matter, microbial processing becomes more important, and microbial products or residues are expected to contribute disproportionately to MAOC. At higher MAOC/SOC, a larger proportion of SOC occurs in mineral-associated form, potentially favoring more direct incorporation of dissolved or root-derived carbon into MAOC. We therefore hypothesize that increasing MAOC/SOC shifts MAOC source enrichment from microbial-derived toward non-microbial carbon relative to bulk SOC.

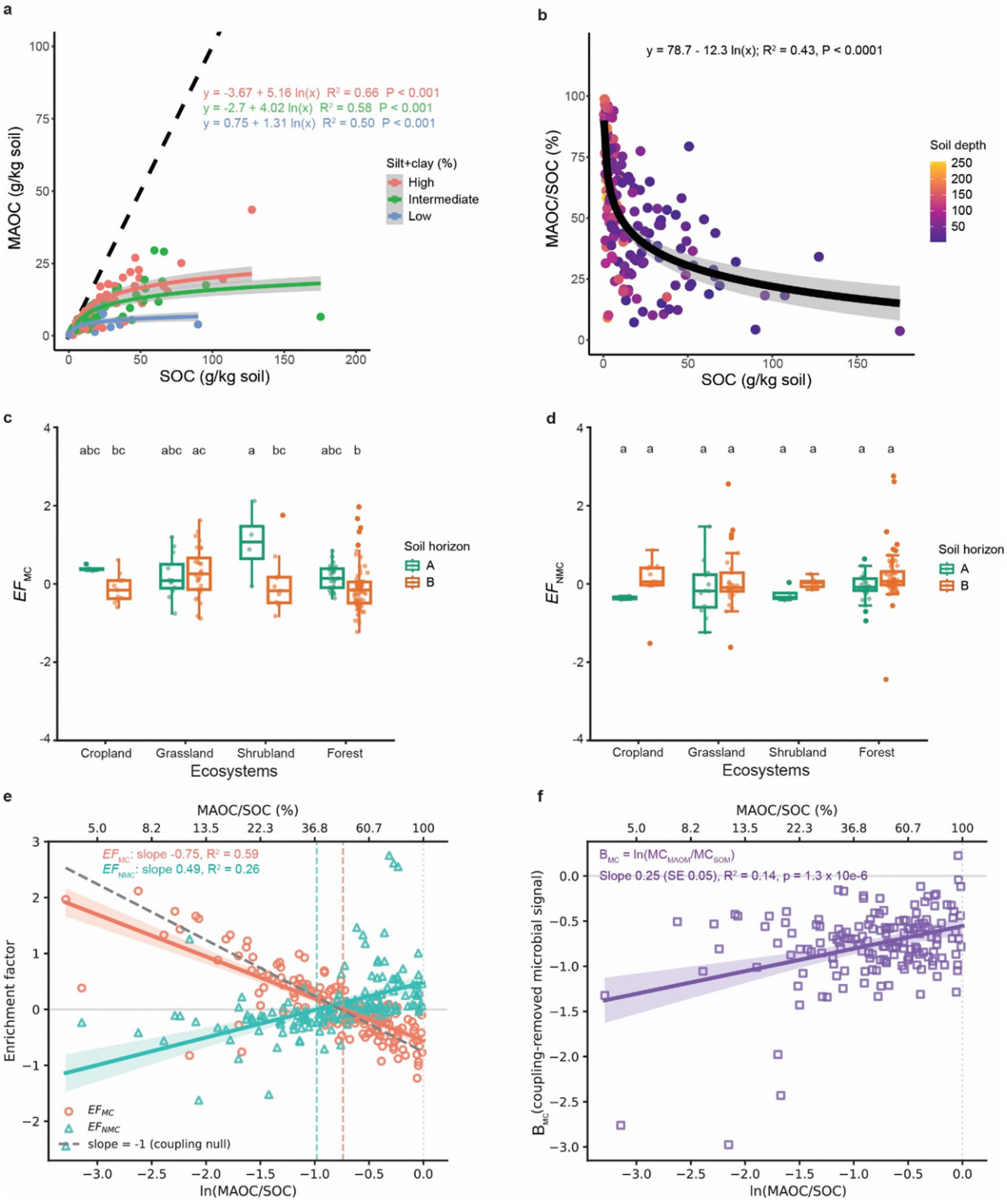


Figure 2. Relationships among mineral-associated organic carbon (MAOC), soil organic carbon (SOC), and enrichment factors of microbial (EF_{MC}) and non-microbial carbon (EF_{NMC}). a, Relationship between MAOC and SOC as a function of silt + clay content. **b,** Relationship between MAOC/SOC and SOC. **c,** EF_{MC} across ecosystems and soil horizons. **d,** EF_{NMC} across ecosystems and soil

horizons. **e,** Relationships of EF_{MC} and EF_{NMC} with ln(MAOC/SOC). **f**, Relationship between the coupling-removed microbial signal B_{MC}, defined as $\ln(MC_{MAOM}/MC_{SOM})$, and ln(MAOC/SOC). In box plots, boxes represent the interquartile range (25th–75th percentiles), centre lines indicate medians, whiskers extend to the range excluding outliers, and points denote outliers. Lowercase letters indicate statistically significant differences ($P < 0.05$). In a, fitted lines correspond to soils with <33% silt + clay (low; blue), 33–66% (intermediate; green), and >66% (high; red). In a, b, e, and f, shaded bands indicate 95% confidence intervals. In e and f, the upper x axis shows the corresponding untransformed MAOC/SOC values (%). In e, the grey dashed line indicates the slope expected from algebraic coupling alone, coloured dashed vertical lines mark fitted EF = 0 transition points, and the grey dotted vertical line marks MAOC/SOC = 100%.

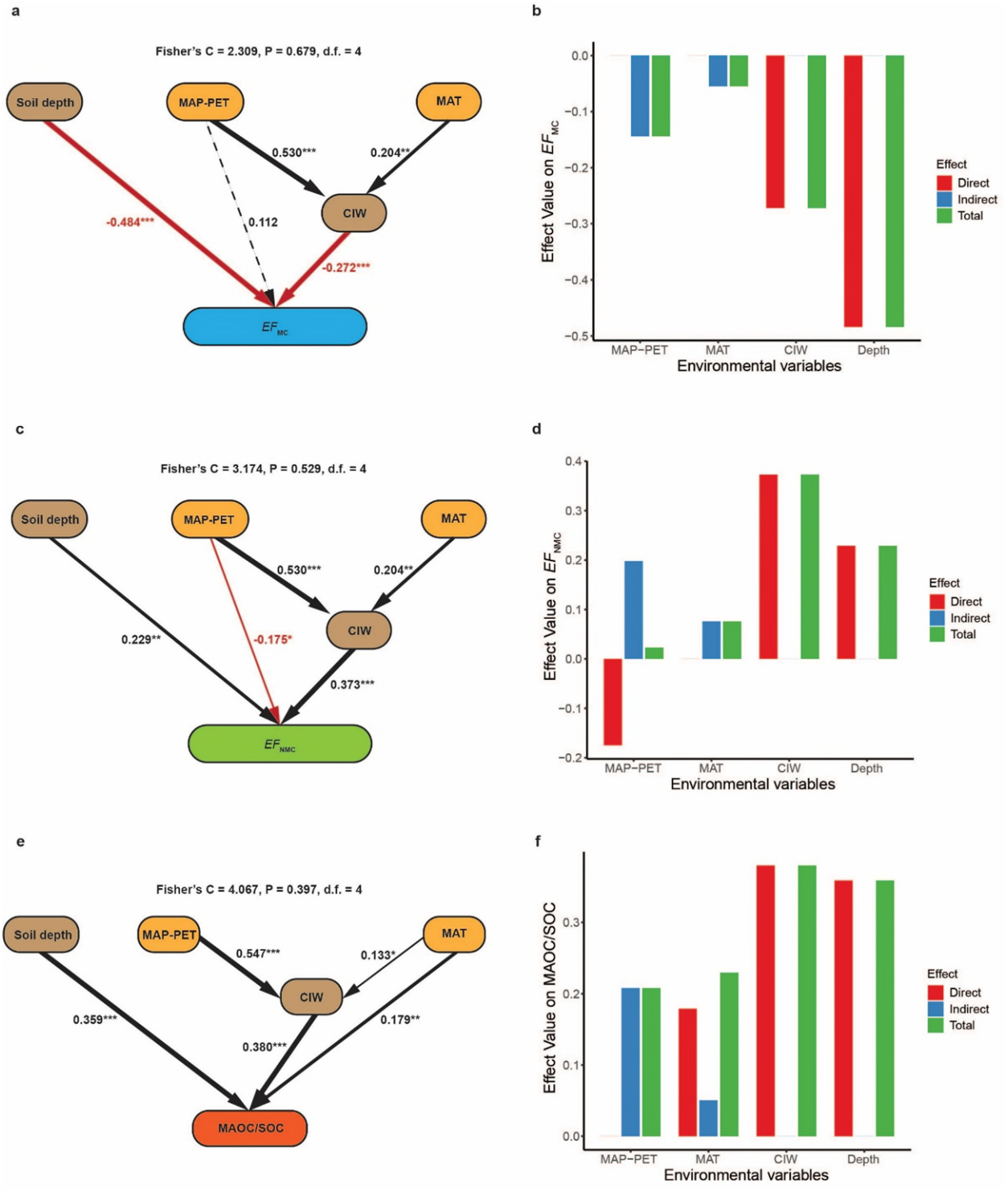


Fig. 3 | Effects of environmental factors on EF_{MC}, EF_{NMC}, and MAOC/SOC. a, Structural equation model (SEM) quantifying direct and indirect effects of environmental variables on EF_{MC}. **b,** The direct, indirect, and total effect of each environmental variable on EF_{MC}. **c,** SEM quantifying direct and indirect effects of environmental variables on EF_{NMC}. **d,** The direct, indirect, and total effect of each environmental

variable on EF_{NMC}. **e,** SEM quantifying direct and indirect effects of environmental variables on MAOC/SOC. **f,** The direct, indirect, and total effect of each environmental variable on MAOC/SOC. In SEMs, solid arrows denote significant paths (black, positive; red, negative); arrow width is proportional to effect strength. Numbers on arrows are standardized path coefficients, with significance denoted as *p < 0.05, **p < 0.01, and ***p < 0.001.

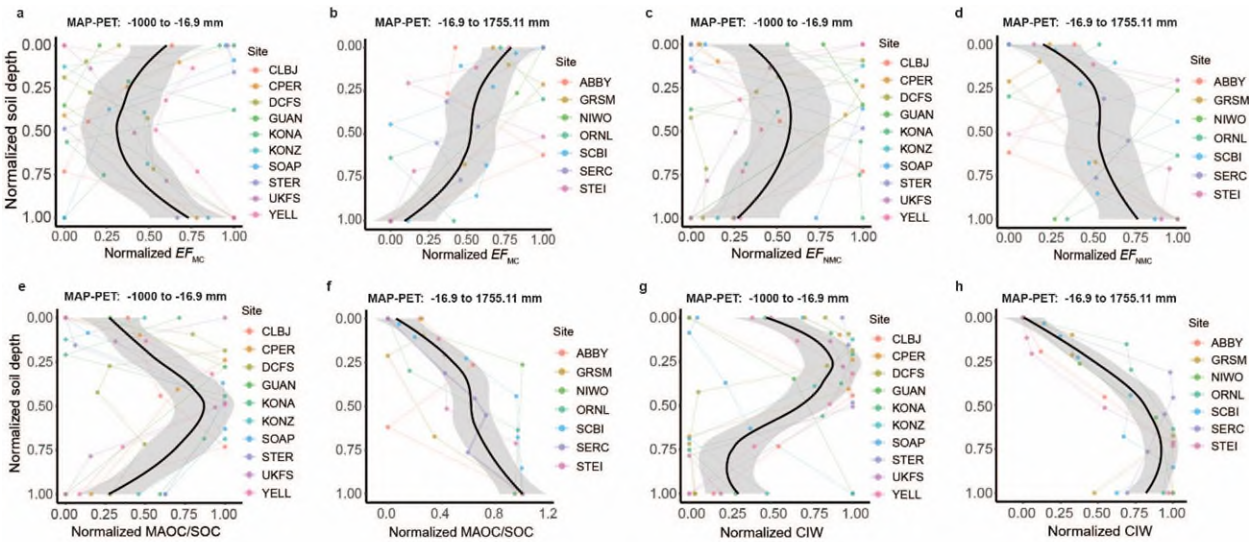


Fig. 4 | Depth-dependent patterns of EF_{MC}, EF_{NMC}, MAOC/SOC, chemical index of weathering (CIW) in arid and humid systems. a, Variation in the EF_{MC} with soil depth in arid systems. **b,** Variation in the EF_{MC} with soil depth in humid systems. **c,** Variation in the EF_{NMC} with soil depth in arid systems. **d,** Variation in the EF_{NMC} with soil depth in humid systems. **e,** Variation in the normalized MAOC/SOC with soil depth in arid systems. **f,** Variation in the normalized MAOC/SOC with soil depth in humid systems. **g,** Variation in the normalized CIW with soil depth in arid systems. **h,** Variation in the normalized CIW with soil depth in humid systems. In each panel, the black curve is a LOESS (locally weighted) regression. The shaded grey band indicates the 95% confidence interval. Points of the same colour denote soil horizons from the same NEON site; same-coloured straight lines connect horizons within a site to indicate within-site depth trajectories.

Supplementary Files

This is a list of supplementary files associated with this preprint. Click to download.

- Supportinginformation.docx